PHYSICAL REVIEW B VOLUME 55, NUMBER 21 1 JUNE 1997-I

Proximity coupling in high-T_c Josephson junctions produced by focused electron beam irradiation

W. E. Booij
IRC in Superconductivity, University of Cambridge, Madingley Road, Cambridge CB3 0HE, United Kingdom and Department of Materials Science, University of Cambridge, Pembroke Street, Cambridge CB2 3QZ, United Kingdom

A. J. Pauza, E. J. Tarte, and D. F. Moore
IRC in Superconductivity, University of Cambridge, Madingley Road, Cambridge CB3 0HE, United Kingdom

M. G. Blamire
IRC in Superconductivity, University of Cambridge, Madingley Road, Cambridge CB3 0HE, United Kingdom and Department of Materials Science, University of Cambridge, Pembroke Street, Cambridge CB2 3QZ, United Kingdom

(Received 23 December 1996)

Using the particular benefits of focused electron beam irradiation (FEBI) junctions, such as on chip modification of the barrier resistivity through controlled variation of the electron fluence and annealing, we show that the conventional model for superconductor–normal-metal–superconductor (SNS) junctions as derived by De Gennes can explain their behavior in great detail. We find that the damage distribution produced by the electron beam has a full width at half maximum of the order of 15 nm and is largely determined by the profile of the electron beam used in the fabrication process. Due to the high defect concentration produced by the electron beam, the barrier material is nonsuperconducting and has a much higher normal-state resistivity than undamaged $YBa_2Cu_3O_{7-\delta}$. From the exponential scaling of the critical current (I_c) with the square root of the resistance (R_n) it is shown that FEBI junctions have a dirty limit SNS character and that the carrier mass in the irradiated material is of the order of m_e. Both the quadratic scaling of I_c with T_c-T close to T_c and the reduced I_cR_n values of the junctions indicate that the SN interface has a soft boundary nature. From the low-temperature scaling of I_cR_n with the ratio of the barrier length and the coherence length we find that the suppressed superconducting gap at the SN interface is approximately 4.5 meV. [S0163-1829(97)01821-3]

I. INTRODUCTION

The fabrication of Josephson junctions in high-T_c superconductors through focused electron beam irradiation (FEBI) is in many aspects unique.[1–3] Whereas the effect of electron irradiation on electrical properties in most materials is marginal, the high-T_c materials are comparatively very sensitive due to their dependence on oxygen ordering. Even electrons with low energies ($\sim$20 keV) have been shown to have some effect on the electrical properties.[2] As a fabrication process for research purposes it is a very elegant technique, allowing the fabrication of a nanometer scale weak link in an unbroken single layer of material. The fact that the film remains unbroken is an enormous advantage in proximity coupled junctions because it allows us to fabricate junctions without interface resistance, which can otherwise severely degrade the maximum current density of Josephson junctions.[4] In contrast to conventional multilayer devices, the nature of the process enables us to accurately adjust both the electrical properties (by varying the electron dose) and the physical dimensions of the barrier on-chip, thereby circumventing the chip to chip reproducibility problems which have long hampered the systematic study of other types of high-T_c Josephson junctions. FEBI junctions show a variation of the critical current with applied magnetic field [$I_c(B)$] which suggests that the current distribution is very uniform.[5]

As a result of extensive studies of electron irradiation effects on high-T_c material (both films and single crystals), the nature of electron-induced damage is relatively well understood.[2,6,7] Through collisions with the lattice the electrons create atomic interstitials and vacancies in the lattice, known as Frenkel defects. Tolpygo *et al.*[2,8] have shown that there is a direct relation between the number of in-plane defects (that act as strong scatterers), the suppression of T_c, and the increase in resistivity in electron-irradiated high-T_c superconducting material. They also found that the creation of in-plane defects has a threshold displacement energy of 8.4 eV [corresponding to an irradiation energy (E_i) of 58 keV],[2] below which incident electrons cannot create in-plane defects.

At the electron energy used in our process (350 keV) the superconducting properties of the irradiated superconducting material can be fully suppressed, resulting in a material that has a nearly temperature independent but rather high resistivity ($\rho_n=10-15\ \Omega\ \mu$m). A further increase of the fluence leads to a further increase of the resistivity and the onset of semiconducting $\rho_n(T)$ behavior. In many ways the effects of electron beam irradiation on the electrical properties of $YBa_2Cu_3O_{7-\delta}$ (YBCO) are similar to cation substitution in the Cu sublattice. However, a clear advantage of electron irradiation-induced defects over substitution experiments is the ability to subsequently reduce the defect concentration in a fabricated sample by annealing.[1,2]

The observation that electron-induced damage in YBCO

 © 1997 The American Physical Society

leads to suppression of T_c and an increase in resistivity suggests a proximity coupled model[9] for FEBI junctions. The damage region, at temperatures above its superconducting transition temperature (T_{cn}), behaves like a normal metal that is proximitized by the superconducting electrodes. Ramp edge junctions with doped YBCO as a barrier[10–12] have properties that can be explained by conventional SNS superconductor–normal-metal–superconductor theory as originally developed by De Gennes and others for BCS-like superconductors.[9,13,14] All these junctions have a barrier material with a finite T_{cn} which means that junctions become strongly coupled $SS'S$ (where S denotes a superconductor and S' denotes a superconductor with a reduced T_c) at low temperatures. A finite T_{cn} also results in junctions with a dramatic exponential-like increase of the critical current (I_c) over a small temperature range above T_{cn}. Similar behavior has been observed in FEBI junctions fabricated using a low electron fluence.[15]

In the following we show that the behavior of FEBI junctions can be explained by conventional SNS theory when the barrier has no such superconducting transition ($T_{cn}=0$). Davidson *et al.*[16] have shown that the shape of the $I_c(T)$ curve of FEBI junctions are like those expected for SNS junctions with rigid boundary conditions. However, from the fact that the junctions showed a low I_cR_n value, they correctly concluded that the order parameter must be suppressed at the SN interface (soft boundary conditions). In earlier work we showed that in FEBI junctions in which the barrier length was increased by scanning the beam over an area (instead of a line scan), I_c had an apparent exponential dependence on barrier length (L), as expected for SNS junctions.[15] However, after annealing the sample, this dependence was no longer found at higher temperatures ($T > 30$ K) where it is expected to work well. In the present paper we will show that the behavior of these FEBI junctions is consistent with SNS theory but that instead of the exponential length dependence, the junctions show an I_c dependence that is consistent with an increase of resistivity of the barrier (due to the increase in electron fluence) rather than an increase in barrier length.

Many objections to the application of conventional SNS theory to high-T_c junctions can be contemplated: the d-wave nature of the order parameter, the complex shape of the Fermi surface, the doped semiconductorlike properties, etc.[17] However, the evidence presented in this paper and others clearly indicates a more than coincidental similarity between these high-T_c junctions and the behavior predicted by conventional SNS theory. Furthermore, until a microscopic theory for the high-T_c materials is developed, comparisons with models derived for BCS-like superconductors provide the only method of gaining insight into the properties of these devices. Concerning the d-wave nature of the high-T_c materials, it should not be forgotten that SNS coupling is a highly directional effect that would obscure many of the complex features of the gap when the junction current flow direction (in c-axis oriented films) is aligned with one of the lobes of the order parameter.[18]

II. THEORY

A. De Gennes dirty limit expression for the critical current

Using microscopic theory for BCS-like superconductors De Gennes[9] was able to obtain an analytical expression for the I_c in long Josephson junctions, for which the coherence length in the normal barrier (ξ_n) is much smaller than the length of the junction (L). More refined derivations of the critical current in SNS junctions by Likharev[13] and Kupriyanov and Lukichev[14] have shown that this expression is reasonably accurate over a wide temperature range.[19] The expression for the critical current in a long SNS junction is

$$I_c(T,L)=\frac{\pi}{4eR_n}\frac{|\Delta_i|^2}{k_bT_c}\frac{L}{\xi_n}\Big/\sinh\left(\frac{L}{\xi_n}\right),\quad 0.3T_c<T<T_c. \tag{1}$$

Here R_n is the normal resistance of the barrier and Δ_i the possibly suppressed gap at the SN interface. De Gennes originally derived this expression for the dirty limit where the coherence length is limited by diffusion (with D_n the carrier diffusion constant): $\xi_{nd}=\sqrt{\hbar D_n/2\pi k_bT}$. The expression for the I_c is actually more generally applicable provided that a suitable expression for the coherence length is used which accommodates, for example, a finite superconducting transition temperature of the barrier (T_{cn}).[20,21] However, the junctions presented in this article received a high electron fluence that fully suppressed the superconducting properties in the irradiated material, rendering $T_{cn}=0$ K.

An important issue to address is whether the barrier is in the clean or dirty limit. When the electronic mean-free path $l_n=m\nu_n/e^2n\rho_n$ is much smaller than the clean limit coherence length $\xi_{nc}=\hbar\nu_n/2\pi k_bT$, the coherence length is diffusion limited and $\xi_n\approx\xi_{nd}$ in Eq. (1). In the dirty limit we therefore expect an I_c which is strongly dependent on the resistivity of the barrier. On the other hand, when $l_n\gg\xi_{nc}$ the barrier is in the clean limit and the coherence length is independent of the resistivity (assuming $T_{cn}=0$): $\xi_n\approx\xi_{nc}$. The determining material parameters are the Fermi velocity (ν_n), the carrier density (n), the carrier's effective mass (m), and the resistivity of the barrier (ρ_n). For 100 keV electron irradiation it was shown that the carrier density of the irradiated material remained nearly unchanged.[2] If we assume that this also holds for the much higher electron energies used in our experiments and we assume that the carrier mass remains unchanged, the Fermi velocity in the barrier is the same as that of undamaged YBCO. Taking into account the strongly anisotropic nature of YBCO we use a two-dimensional (2D) expression to find the Fermi velocity in the CuO sheets:[22] $\nu_n=(h/2\pi m)(2\pi n|c|)^{1/2}$, where $|c|$ denotes the c-axis lattice parameter of YBCO ($|c|=1.16$ nm). Using the carrier properties of optimally doped YBCO [$n=5\times10^{27}$ m^{-3} and $m=5m_e$ (Ref. 23)] we obtain $\nu_n=1.4\times10^5$ m/s. Using this value for the Fermi velocity and a typical minimum resistivity of our barriers of $\rho_n=3\ \Omega\ \mu$m one can easily show that $\xi_{nc}\gg l_n$ so that the coherence length is dominated by the dirty limit expression (2D) $\xi_n\approx\xi_{nd}=(\xi_{nc}l_n/2)^{1/2}$. As we will see later, the carrier effective mass in FEBI barriers is found to be much smaller than that of optimally doped YBCO, typically of the order of m_e. This makes the criterion $\xi_{nc}\gg l_n$ easier to fulfill because it leads to an increase of ξ_{nc} whereas l_n remains the same. We can obtain a relation between the ratio L/ξ_{nd} and the R_n of the barrier using the expression for l_n and ξ_{nc} in terms of ν_n and expressing the resistivity of the barrier in terms of R_n, L, and A the cross-sectional area $\rho_n=R_nA/L$:

$$L/\xi_{nd}(T)=[(2e^2mk_bT/\hbar^3|c|)LR_nA]^{1/2}. \quad (2)$$

At a given temperature the magnitude of the critical current in an SNS junction is strongly determined by the exponential dependence on the ratio L/ξ_{nd}. As a good approximation to De Gennes' expression at a fixed temperature we can therefore write $I_cR_n \propto e^{-L/\xi_{nd}}$. For junctions with constant resistivity but varying barrier length this equation predicts the well-known exponential dependence of I_cR_n with length. If, however, we keep the barrier length constant and instead vary the resistivity, as is easily done by varying the fluence for FEBI junctions, Eq. (2) predicts an exponential dependence of I_cR_n on the square root of the resistance when the junctions are in the dirty limit:

$$I_cR_n \propto e^{-\alpha(R_n)^{1/2}}, \quad (3)$$

where the parameter α can be found as the slope of a line in a $\ln(I_cR_n)$ versus $(R_n)^{1/2}$ plot and is given by $\alpha=\sqrt{(2e^2mk_bTLA)/(\hbar^3|c|)}$.

B. Soft or rigid boundary conditions

One consequence of the proximity effect is the establishment of a critical current through the barrier. Another consequence is the suppression of the superconducting gap in the electrodes $\Delta_i=\delta_i\Delta_\infty$, when the electronic properties of the barrier and electrodes are similar (soft boundary conditions). Here Δ_∞ denotes the value of the BCS gap far away from the junction and δ_i denotes the suppression factor. An important effect of this phenomenon is the reduction of the I_cR_n product of such a well-matched SNS junction. A key parameter determining the gap suppression, which is a measure of the electrode/barrier matching, is[9,19] $\gamma=(N_n\rho_s/N_s\rho_n)^{1/2}$, where N_i is the density of states. Once a value for γ has been found the suppression factor (δ_i) can be calculated using[19]

$$\delta_i^2=1+\left(\frac{\xi_{sd}}{b_i}\right)^2-\left[\left(\frac{\xi_{sd}}{b_i}\right)^4+2\left(\frac{\xi_{sd}}{b_i}\right)^2\right]^{1/2},$$

$$\text{with } \frac{\xi_{sd}}{b_i}=\frac{\pi}{2}\gamma\left(\frac{T}{T_c-T}\right)^{1/2}. \quad (4)$$

Here, ξ_{sd} is the Ginzburg-Landau penetration depth in the electrodes and b_i is known as the extrapolation length. If γ is of the order 1, the suppression of the gap is significant ($\delta_i^2 \approx 0.1$) especially close to T_c. The temperature range where Eq. (4) can be applied is similar to that in which Eq. (1) is valid, as a consequence of using Ginzburg-Landau theory in its derivation.

Rigid boundary conditions correspond to the case in which $\gamma \ll 1$, leading to a negligible suppression of the electrodes' gap and optimal I_cR_n values. Assuming that the density of states of the barrier is approximately the same as that of the electrodes, the suppression of the superconducting gap is completely determined by the ratio of the resistivities. Looking in detail to the scaling of the I_c with (T_c-T) close to T_c provides one with an experimental way of determining whether a SNS junction has soft or rigid boundary conditions. Whereas the global $I_c(T)$ behavior of SNS junctions is largely determined by the exponential-like behavior of the $\sinh(L/\xi_n)$ term, the $I_c(T)$ behavior close to T_c is determined by the strong temperature dependence of Δ_i. For rigid boundary conditions this quantity is equal to the BCS gap Δ_∞, which scales as $(T_c-T)^{1/2}$. Therefore rigid boundary conditions will lead to a linear dependence of I_c on (T_c-T). In the case of soft boundary conditions (with $\gamma>0.2$) the added temperature dependence of the suppression factor close to T_c, $\delta_i^2 \propto (T_c-T)/T$ leads to $I_c \propto (T_c-T)^2$.[19]

C. Critical currents at low temperatures

At low temperatures the De Gennes expression for the I_c can no longer be used. Microscopic theories such as Likharev's calculations for long junctions with rigid boundary conditions predict a much slower temperature variation at low temperatures than that expected from Eq. (1). For $T<0.4T_c$ these theories typically predict a linear region than rounds off at low temperatures $T<0.1T_c$.[13] Using Likharev's results, Delin and Kleinsasser[19] derived an expression for the I_cR_n at low temperatures that is only dependent on the value of the superconducting gap and the ratio $L/\xi_{nd}(T_c)$:

$$I_cR_n=\frac{29\Delta_\infty}{e}\left(\frac{\xi_{nd}(T_c)}{L}\right)^2, \quad (5)$$

where $T \leqslant 0.05T_c$ and $L \geqslant 6\xi_{nd}(T_c)$. For soft boundary conditions no such expression for the critical current at low temperatures exists. However, numerical calculations by Kupriyanov and Lukichev show that the I_cR_n product at low temperatures decreases with increasing values of γ.[14] For a constant value of γ the effective gap value of the soft boundary SNS junctions will simply be reduced and we expect that a relation very similar to Eq. (5), with Δ_∞ replaced by Δ_i, will hold.

III. EXPERIMENTAL PROCEDURE

A. Experimental setup

For junction fabrication we used high-quality 200-nm-thick c-axis oriented $YBa_2Cu_3O_{7-\delta}$ films grown by laser ablation on $LaAlO_3$. Tracks with a width of 1.8 μm were then patterned by optical lithography and argon ion milling at 500 eV on a water-cooled rotating stage. The tracks were carefully aligned with the crystal a or b axis. The T_c of the film was measured before and after patterning and was found to be unchanged at 90.5 K. Before the FEBI process we measured the current density (J_c) of the tracks to check the processing and film quality. The critical current density of the tracks for the sample presented in this article was 2.6×10^{10} A/m^2 at 77 K with a minimum-to-maximum deviation of 10% (nine tracks). The tracks were irradiated in a JEOL 4000EX scanning transmission electron microscope (STEM) at an acceleration voltage of 350 kV and a magnification of 10 000. The STEM was specially modified for electron beam write processes and is located on a vibrationally isolated platform. The tracks were exposed using a computer controlled positioning and blanking system with a positioning accuracy better than 1 nm (at the selected magnification of 10 000). Before irradiation, a thin (<5 nm) gold layer was deposited on top of the sample to avoid charging problems.

The current-voltage (IV) characteristics of the junctions were measured using a dip probe that fits into a standard liquid Helium Dewar. The temperature of the copper block on which the sample was mounted could be controlled within 50 mK. The sample was surrounded by a μ-metal shield that reduces the ambient field to less than 320 nT (at room temperature). Electrical noise was carefully minimized by filtering all leads going down to the sample. For resistively shunted junction (RSJ)-like IV characteristics the I_c and R_n were found from V^2 vs I^2 plots; the advantage of this method is that even thermal-noise-rounded IV characteristics can be reliably analyzed. Junctions in the large limit have a non-RSJ-like IV characteristic, in which case the I_c was found using a finite voltage criterion of 0.5 μV and the R_n was determined at high bias currents ($5\times I_c$). At temperatures at which the junction have no I_c, the R_n of the junctions was measured using a 10 μA ac bias. The critical current density of FEBI junctions is not self-field limited due to their planar geometry,[24] therefore comparison of the measured I_c with calculated values is not bound to any upper limit as was found to be the case for sandwich-type SNS junctions.[25]

B. Electron beam profile and implications for the damage spread

In estimations of the barrier length of FEBI junctions, it is often assumed that the incident electron beam can be regarded as pointlike, with the damage spread resulting entirely from scattering of the incoming electrons within the irradiated material. Monte Carlo calculations for 350 keV electrons being scattered in a 200-nm-thick YBCO film result in a strongly peaked non-Gaussian distribution of scattering events, which suggests that 50% of the damage is confined to a 4-nm-wide region. A number of experiments[1,15,26] indicate that the damage spread occurs on a larger scale and does not increase much with increasing film thickness.

An experimental value for the beam spread can be obtained from an experiment, in which the beam is periodically turned on and off during a line scan. This study[15,26] indicates that damage overlap for the small aperture in a 200-nm film occurs on a length scale of 10 to 20 nm. A confirmation that scattering of the incident electrons has an insignificant effect on the damage distribution is obtained from a study of the scaling of the electrical properties of FEBI junctions, which indicates that the Josephson current and quasiparticle cross section are identical.[1] Assuming an SNS nature for these junctions, a barrier which widens with increasing film depth would lead to a strong concentration of the Josephson current at the position of the smallest barrier length. These experiments therefore lead to the conclusion that the damage spread in a 200-nm-thick film is not determined by internal scattering of the electrons but by the intrinsic spread of the incoming beam. Often quoted optimal spot diameters of STEM's used in irradiation experiments are on the order of 3 nm.[16,27,28] However, such a small spot size can only be obtained at low beam currents (when a small condenser aperture and spot size are selected) and optimal beam alignment and focusing. The assumption that the length of the barrier is equal to the optimal spot size (3 nm) at the much higher beam currents used in FEBI experiments is therefore highly optimistic and leads to unphysical values for the coherence length in the barrier.[16]

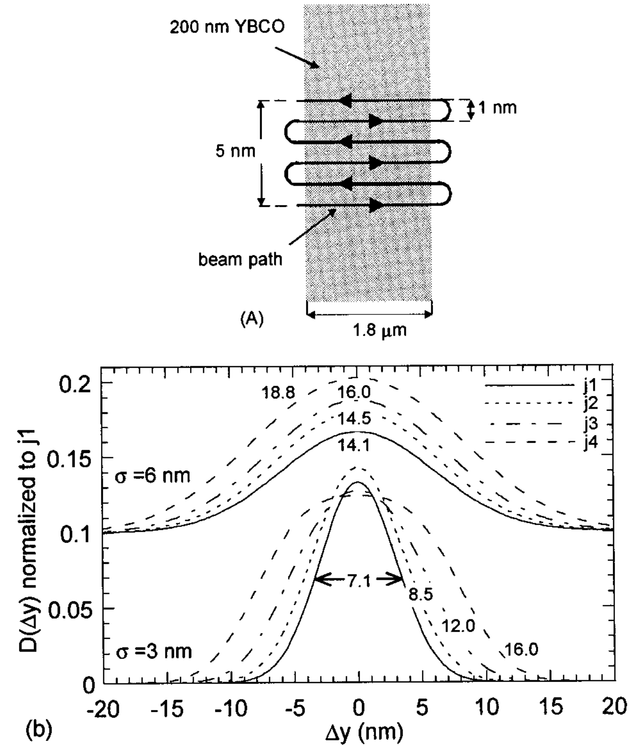

FIG. 1. (a) The beam path of $j2$, which is widened by 5 nm while the electron dose was increased by a factor of 1.33. For junctions 3 and 4 the beam was scanned over 10 and 15 nm while increasing the electron dose by a factor of 1.66 and 2.0, respectively. (b) The calculated damage distribution $[D(\Delta y)]$ of junctions 1, 2, 3, and 4 assuming a Gaussian distribution for an unwidened junction. The fabrication procedure results in widening of the barrier when the defect distribution has a low spread ($\sigma=3$ nm). For a moderate defect spread ($\sigma=6$ nm) the procedure results in an effective increase of defect concentration without significantly increasing the barrier length [the $D(\Delta y)$ has been offset by 0.1]. The FWHM in nm of each distribution is indicated.

The use of a large condenser aperture (200 μm in our STEM) and associated high beam currents, in order to minimize the irradiation time, can result in junctions with strongly reduced I_cR_n products due to the large intrinsic non-Gaussian spread of the electron beam.[27,28] The use of a 100-μm condenser aperture results in greatly improved junctions and proven reduction of the spatial damage spread.[15] However, these values are still large when compared to the damage spread expected from scattering within the irradiated YBCO film, indicating that further improvement is possible.

Based on the beam modulation experiment described earlier, we estimate the barrier length to be approximately 15 nm. Using this estimate we can calculate the effective fluence of a 1.8-μm-wide junction with an $I_c\approx 10\ \mu A$ at 60 K to be 6.33×10^6 C/m^2. In order to further clarify the nature of our FEBI junctions the barrier length of junctions was increased by scanning the beam over a narrow region instead of a line while intending to keep the fluence approximately constant [Fig. 1(a)]. Whereas the first junction ($j1$) was pro-

duced by a line scan with a total line dose of 0.095 C/m the subsequent junctions ($j2$,$j3$,$j4$) were widened by 5, 10, and 15 nm in the y direction as shown schematically in Fig. 1(a) while the total dose was consecutively increased by a factor 1.33, 1.66, and 2. If we assume that the damage spread resulting from a line scan is approximately Gaussian with a standard deviation σ, we can calculate the effect of the widening and dose increase on the damage distribution $[D(\Delta y)]$. We present the case for a small ($\sigma=3$ nm) and moderate ($\sigma=6$ nm) spread in damage in Fig. 1(b). For the $\sigma=3$ nm case the combined effect of widening and increasing dose is to widen the barrier significantly while the maximum damage concentration remains approximately constant.

If a moderate damage distribution with $\sigma=6$ nm is assumed, the result is completely different. In this case the beam is scanned over a length scale comparable to the full width at half maximum (FWHM) of the damage distribution resulting in a damage distribution with only slightly increased FWHM but increased damage concentrations. So, whereas the $\sigma=3$ nm case will lead to junctions with similar resistivities but increased barrier length, the $\sigma=6$ nm case will result in junctions with similar barrier lengths but increased resistivity. The two different cases result in a very different scaling behavior of the I_c. Note that from the beam modulation experiment we expect damage overlap to occur between 10 and 20 nm, indicating that the experiment is most likely to result in a damage spread close to that given by the $\sigma=6$ nm case.

By annealing the sample in air at four different temperatures ($a1$, $a2$, $a3$, and $a4$ corresponding to 323, 353, 388, and 431 K) for typically an hour, the barrier properties were modified. Through annealing and subsequent characterization of the junction properties, barriers with a wide variety of electrical properties could therefore be studied on a single chip.

IV. RESULTS AND DISCUSSION

A. Scaling of I_c with L or R_n

On a single 5×5 mm chip nine junctions with different barrier properties were fabricated. Although all nine junctions were available for measurement, only the first four junctions had measurable critical currents at all stages of annealing. To keep the number of measurements tractable we restricted the measurements to the first four junctions ($j1$ to $j4$). This procedure resulted in a set of 16 complete measurements of junctions with different barrier properties.

All the junctions were of a high quality showing a regular variation of the critical current with applied magnetic field and full suppression of the I_c when the junctions were in the small limit. In the small junction limit all the IV characteristics could be described using the RSJ model. At high critical current densities, IV characteristics were observed which showed a large excess current and, at very low temperatures ($T<10$ K) small hysteresis effects ($<5\%$ of I_c). A crossover to flux flow behavior was observed at low temperatures ($T<50$ K) for junctions 1 and 2 after anneal 4, when these junctions had very high critical current densities ($J_c>10^6$ A/cm^2). We believe that this behavior is simply a result of the small value of L/ξ_{nd} of these junctions at these temperatures and is not caused by a superconducting transition of the barrier. Unlike junctions with barriers that undergo a superconducting transition, it was found that the critical current of these junctions could still be partially suppressed ($\sim30-50\%$) by a magnetic field which normally results in the first minimum (B_0).

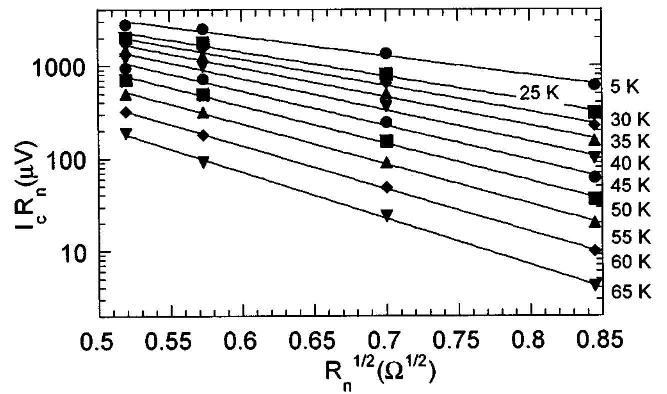

FIG. 2. The scaling of I_cR_n with $(R_n)^{1/2}$ for the four junctions is clearly exponential over a wide temperature range, as is expected for a dirty limit SNS junction. The data shown here were taken after anneal stage 3.

The dependence of I_cR_n on the junction parameters L and R_n represents the most direct method to verify whether the FEBI junctions have an SNS character. Although the I_c of the junctions after the first anneal stage and at low temperatures shows an exponential dependence on L,[15] we now believe that this dependence is coincidental. There are a number of reasons why an exponential dependence is not expected. (a) The barrier length used in the $I_c(L)$ plot was simply taken as the sum of the unwidened barrier length (15 nm) and the widening in the direction normal to the junction (multiple of 5 nm). As was shown in Fig. 1 it is unlikely that this yields a correct estimate of the barrier length when we are dealing with a (Gaussian) defect distribution. (b) The I_c data of the same junctions after subsequent annealing stages no longer show the exponential dependence on L. (c) At low temperatures Eq. (1), from which the exponential I_c dependence is derived, is not valid.

For the damage spread expected in these junctions (FWHM$\sim$10–20 nm) the experiment should instead lead to an effective increase of fluence rather than a increase of the barrier length (see Fig. 1). We therefore expect from Eq. (3) that the I_cR_n at temperatures above $0.3T_c$ for fixed barrier length depends exponentially on the square root of R_n of the junctions. As will be shown below, the R_n of the junctions is well defined and nearly temperature independent. In Fig. 2 it is shown that all the measured I_c values after every anneal stage follow this dependence. The exponential fits describe the data quite well even at low temperatures.

From the slope of the lines in Fig. 2 according to Eq. (3) the parameter $\alpha=\sqrt{(2e^2mk_bTLA)/(\hbar^3|c|)}$ can be found. This expression predicts a linear relation between α^2 and the temperature T, a dependence that is verified in Fig. 3 for anneals 1, 2, and 3. Because Eq. (3) is valid only at temperatures higher than approximately 30 K we fitted α^2 for $T>30$ K with a straight line through the origin. The fits are good especially for anneal 1 and 2. Deviations from the expected linear behavior may be a result of the approximate

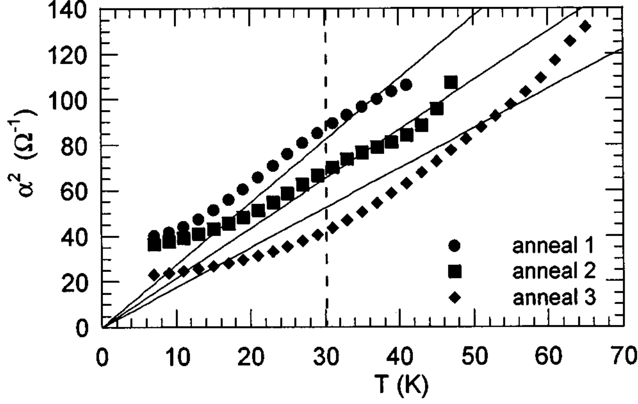

FIG. 3. The squared slope of the lines (α^2) in Fig. 2 is approximately proportional to the temperature. Only the data above $T = 30$ K was used for the line fit. Below 30 K the exponential scaling is not expected to give a reliable value for α^2 and a significant deviation from the line fits is observed. Annealing causes a decrease of the slope of the fits.

nature of Eq. (3), for which both L/ξ_{nd} and Δ_i in De Gennes' I_c expression were neglected. This possibly also explains why the α^2 data after anneal 4 (not shown) could not be fitted with a line through the origin, although the junctions still showed an exponential dependence of I_c with $R_n^{1/2}$ to some degree.

As will be shown below the FEBI junctions are best described by soft boundary conditions, which will change the temperature dependence of the I_cR_n product significantly at temperatures close to T_c. At low temperatures α^2 is no longer proportional to T, due to the much slower rise of the I_cR_n product than that predicted by Eq. (3). Delin and Kleinsasser have shown that, as a consequence, the dirty limit coherence length as found from an exponential fit at low temperatures is significantly lower than the true value. Similar behavior is observed in Fig. 3, where the measured α^2 at low temperatures is larger than the expected linear dependence. From the slope of the line fits in Fig. 3 the parameter $\beta = (2e^2mk_bLA)/(\hbar^3|c|)$ can be obtained, which clearly decreases with increasing anneal temperature (Table I). This decrease may be due to a decrease in the carrier effective mass m and/or a decrease of the barrier length L. Annealing studies of the beam modulation junctions[26] reveal that the damage overlap does not change significantly, suggesting that the barrier length does not change by annealing. Let us therefore consider the case where $L = 15$ nm and the decrease in β is due to a decrease of m. This results in m decreasing from $1.07m_e$ for anneal 1 to $0.68m_e$ for anneal 3 (Table I). This value is rather small when compared with the carrier mass in undamaged YBCO $m \approx 5.0m_e$ (Ref. 23) and suggests that the FEBI process leads to delocalization of the carriers in YBCC. The carrier concentration n does not appear in the above expression for β because a 2D expression was used for the Fermi velocity. Had we used a 3D expression instead, the decrease in β could also be explained by a decrease in carrier concentration as was considered by Davidson *et al.* for their FEBI junctions.[16]

B. The magnitude of the critical current and De Gennes expression

From the above discussion we can conclude that the scaling of I_cR_n with R_n is consistent with that expected for an SNS junction in the dirty limit. We now consider the magnitude of the critical current as found from De Gennes' expression for an SNS junction in the dirty limit [Eq. (1)]. A representative selection of the $R_n(T)$ and the $I_c(T)$ of measurements of the FEBI junctions is shown in Fig. 4.

The solid lines in Fig. 4(a) represent fits to the $I_c(T)$ data using De Gennes' expression [Eq. (1)] with soft boundary conditions. For these fits two parameters are required. (a) The electronic matching parameter $\gamma = (N_n\rho_s/N_s\rho_n)^{1/2}$, which was calculated with the assumption that the density of states of the irradiated material is similar to that of undamaged YBCO. We took the resistivity of the electrode material to be temperature independent at 1 Ω μm. The barrier resistivity was calculated from the average R_n of the junction, $A = 3.6 \times 10^{-13}$ m^2 and $L = 15$ nm. (b) The parameter $L/\xi_{nd}(T_c)$ was varied to obtain the best possible fit. Both parameters are shown in Table II for all the junctions. Because De Gennes expression is only valid for $T > 0.3T_c$, we only fitted the I_c data above 30 K. The values obtained for the ratio $L/\xi_{nd}(T_c)$ from the fits are quite reasonable and show the expected trend with both increasing fluence and increasing anneal temperature. The low-temperature $I_c(T)$ behavior is qualitatively consistent with Likharev's model for rigid SNS junctions. It is interesting to note that the shape of the normalized $I_c(T)$ curves remains approximately the

TABLE I. β and $\chi = \beta T_c$ from line fits to Fig. 3 and Fig. 5 after the different anneal stages shown and the derived carrier mass m normalized by the electron mass m_e using $L = 15$ nm.

Anneal No.	Anneal	β (slopes Fig. 3) $[(\Omega\ \mathrm{K})^{-1}]$	m/m_e (from β)	χ (slopes Fig. 5) (Ω^{-1})	m/m_e (from χ)
Anneal 1	1 h @323 K	2.73	1.07	318.4	1.37
Anneal 2	2 h @353 K	2.17	0.85	229.5	0.99
Anneal 3	1 h @388 K	1.75	0.68	170.3	0.73
Anneal 4	1 h @431 K			142.1	0.61

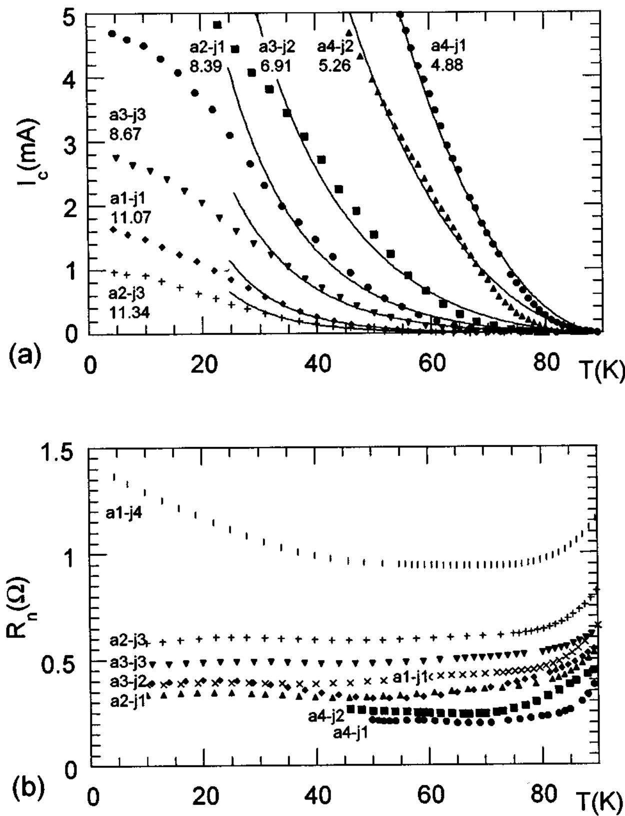

FIG. 4. (a) The $I_c(T)$ measurements for a number of junctions (as symbols) and the De Gennes fit as a full line. Both the $I_c(T)$ and $R_n(T)$ curves are marked by an identifier that lists the anneal and junction number. The fitting parameter $L/\xi_{nd}(T_c)$ is listed below the junction identifier. (b) The $R_n(T)$ curves for the same junctions as shown in (a), showing that the R_n is nearly temperature independent. The junction with the highest resistance ($a1$-$j4$) shows a semiconductinglike increase of $R_n(T)$. The $I_c(T)$ of this junction is not shown in (a) as it would not significantly deviate from the x axis on the scale used.

same for all the junctions for which we could measure $I_c(4.2\ \mathrm{K})$ (<15 mA).

Most of the $R_n(T)$ curves in Fig. 4(b) show a nearly temperature-independent junction resistance, as is expected for a metal that is dominated by impurity scattering. The junction with the highest resistance shows a semiconducting $R_n(T)$ behavior. For calculation of the I_c using Eq. (1) an accurate value of the R_n is required. The high-temperature R_n data are compromised because they are near to the transition temperature of the electrode and are therefore ignored. For the high R_n junctions the semiconducting behavior at low temperatures can change the average R_n significantly. The R_n value used for calculation of the I_c (as listed in Table II) is thus obtained by averaging the $R_n(T)$ over the temperature range from 40 to 70 K. Using $A=3.6\times10^{-13}\ \mathrm{m}^2$ and $L=15$ nm we can calculate the resistivity of the barrier of junction 4 after anneal 1 to be 22.6 $\Omega\ \mu$m, which is significantly higher than that of the undamaged material (1 $\Omega\ \mu$m).

As a result of fitting De Gennes' expression to the $I_c(T)$ data, we obtained $L/\xi_{nd}(T_c)$ [Fig. 4(a)] which according to Eq. (2) is proportional to $(R_n)^{1/2}$. This relation allows us to check whether the fitting of the I_c with the De Gennes expression is internally consistent with the analysis of the I_cR_n scaling with R_n as presented in Figs. 2 and 3. In Fig. 5 it is shown that the $L/\xi_{nd}(T_c)$ data after the same anneal step are well described by a straight line through the origin confirming the dependence expected for an SNS junction in the dirty limit. Furthermore, the fits show the same trend of a decreasing slope with increased anneal temperature as found in Fig. 3. In fact, the slopes obtained from Fig. 5 (defined as χ) should be related to the quantity β found earlier, in the following way: $\chi=\beta T_c$. In contrast to the direct scaling analysis of I_c with R_n we now also find the appropriate scaling for the data after anneal 4. This is because we have now properly taken into account the soft boundary conditions of the junctions that significantly decreases the I_c close to T_c. The values for χ are shown in Table I for all four anneals. Using the same value for the barrier length as before, $L=15$ nm, the effective carrier mass can again be calculated (Table I). The resulting values for m/m_e are slightly higher than those found from the scaling of I_cR_n with R_n. This is possibly a consequence of the approximations made in deriving Eq. (3) as discussed earlier and/or the rather approximate value of γ as used in the fits of Fig. 4(a). From the absolute values of the ratio $L/\xi_{nd}(T_c)$ as listed in Table II and the assumption that the barrier length is approximately 15 nm we find that the value of $\xi_{nd}(T_c)$ varies between 0.85 nm for the most heavily damaged junction and 3.3 nm for the junction that received the lightest fluence. These values are rather similar to those obtained for the doped ramp edge junctions[10–12,19] and significantly larger than the a,b-direction unit-cell dimensions. Because the barrier length is not accurately known (we estimate a possible error of 5 nm) the derived values of both $\xi_{nd}(T_c)$ and m are relatively inaccurate. Still, such an error margin does not result in unphysical values for $\xi_{nd}(T_c)$.

C. Soft or rigid boundary conditions—the scaling of I_c with (T_c-T)

Although rigid boundary conditions require one parameter less ($\gamma=0$) than soft boundary conditions and are therefore preferable for fitting, fits using rigid boundary conditions were particularly unsatisfactory at temperatures close to T_c. This is illustrated in Fig. 6 by the dashed line representing a rigid boundary fit to the junction with the highest operating temperature. For barriers with a higher resistivity that did not show a measurable critical current at high temperatures there was no significant difference in the quality of fits using either soft or rigid boundary conditions.

The fact that soft boundary conditions better describe the behavior of the FEBI junctions is confirmed by studying the scaling of I_c with (T_c-T) close to T_c. Taking the I_c data of the junction with the highest operating temperature ($j1$ anneal 4) and using $T_c=90.5$ K, Fig. 6 shows that the I_c is much better described by a fit using De Gennes expression in combination with soft boundary conditions. The fit using rigid boundary conditions fails to match the slow increase of I_c close to T_c. The inset in Fig. 6 shows the scaling of I_c

TABLE II. Junction and SNS fitting parameters after the different anneal stages. R_n is obtained by averaging the 40–70 K junction resistance and is used for calculating γ. $L/\xi_{nd}(T_c)$ is found from the fits in Fig. 4(a) using De Gennes' expression. The I_cR_n at $T=4.2$ K is obtained directly from the IV characteristic of the junctions.

Anneal	Junction	R_n av. (Ω)	$L/\xi_{nd}(T_c)$	γ	I_cR_n(μV) 4.2 K
Anneal 1	$j1$	0.409	10.88	0.32	633
1 h	$j2$	0.550	13.02	0.28	414
@323 K	$j3$	0.715	15.14	0.24	172
	$j4$	0.942	17.53	0.21	85
Anneal 2	$j1$	0.337	8.17	0.35	1598
2 h	$j2$	0.412	9.02	0.32	1504
@353 K	$j3$	0.596	11.48	0.26	562
	$j4$	0.844	14.42	0.22	238
Anneal 3	$j1$	0.270	6.3	0.39	2785
1 h	$j2$	0.328	6.91	0.36	2479
@388 K	$j3$	0.491	8.83	0.29	1354
	$j4$	0.714	11.47	0.24	608
Anneal 4	$j1$	0.207	4.52	0.45	
1 h	$j2$	0.250	5.26	0.41	
@431 K	$j3$	0.310	6.72	0.37	
	$j4$	0.448	8.45	0.31	1451

with $(T_c-T)^2$ which is well described by a straight line through the origin. We expect an exponent approaching 2 for soft boundary conditions with $\gamma>0.2$.[19] As can be seen in Table II, the value for γ for this particular junction is 0.45 which satisfies the condition $\gamma>0.2$ discussed above.

D. I_cR_n scaling at $T=4.2$ K

Another test of the SNS nature of the FEBI junctions is provided by the relation between the obtained fitting parameters $L/\xi_{nd}(T_c)$ and the I_cR_n products of the junctions at very low temperatures. The I_cR_n products at 4.2 K are shown in Table II for a number of junctions. Due to the very high

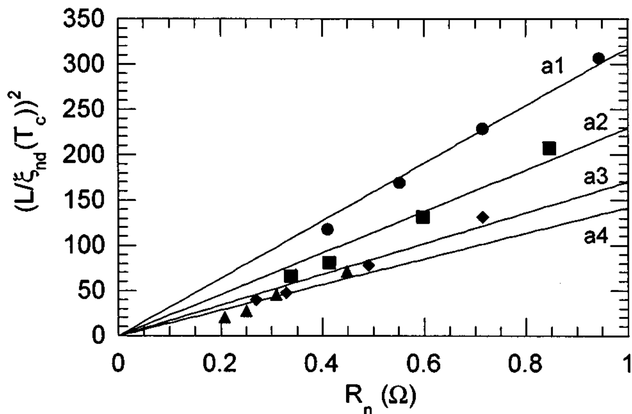

FIG. 5. The scaling of the fitting parameter $[L/\xi_{nd}(T_c)]^2$ with the average junction resistance R_n. The junctions at the same anneal stage are fitted with a straight line through the origin. Increasing anneal temperature results in a decrease of the slope of these lines.

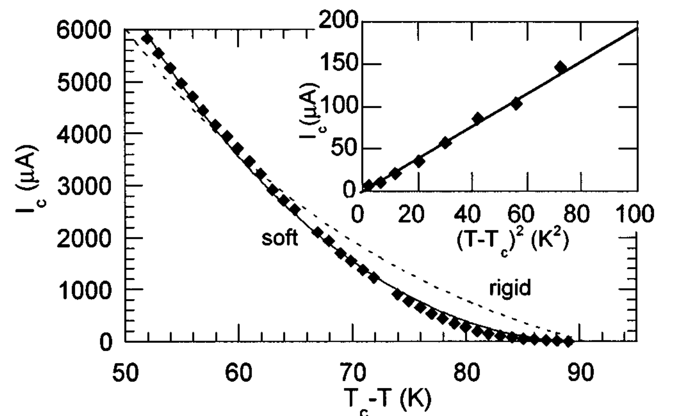

FIG. 6. The I_c data of junction 1 after anneal stage 4 close to the T_c of the film. De Gennes' expression using soft boundary conditions results in a much better fit than when rigid boundary conditions are used. The inset clearly shows that $I_c \propto (T-T_c)^2$ as is expected for soft boundary conditions.

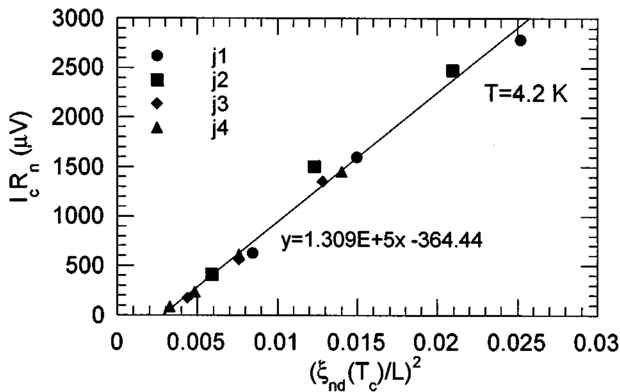

FIG. 7. The I_cR_n product of a number of junctions as a function of $[\xi_{nd}(T_c)/L]^2$ can be fitted with a straight line. In contrast to what is expected from theory for rigid SNS junctions, these junctions cross the $I_cR_n=0$ axis at a finite value for $L/\xi_{nd}(T_c)$. The slope gives the effective superconducting gap.

current densities of some of the junctions after anneal 4 we could not measure the I_cR_n products of these junctions at low temperatures. For SNS junctions with rigid boundaries, Likharev's theory predicts a simple relation, Eq. (5), between the I_cR_n product and the ratio $L/\xi_{nd}(T_c)$. Although the FEBI junctions are better modeled using soft boundary conditions, it is expected that a relation similar to Eq. (5) should hold for these junctions as the effect of soft boundary conditions is to suppress the effective gap value.[14] As we can see in Table II the matching parameter γ does not vary very much between the different junctions and therefore we expect that the effective gap value is similar for all the junctions.

A plot of all the available I_cR_n(4.2 K) products versus $[\xi_{nd}(T_c)/L]^2$ is shown in Fig. 7. The data can clearly be fitted with a straight line. However, the line does not go through the origin as predicted by Eq. (5). The finite value of the $L/\xi_{nd}(T_c)$ ratio for $I_cR_n=0\ \mu$V means that there is a cutoff ratio for $L/\xi_{nd}(T_c)=17.8$ above which there is no measurable I_cR_n product at low temperatures. Equation (5) furthermore predicts that the slope of the line is determined by the superconducting gap in the electrodes far from the barrier. If we use the BCS gap for YBCO, $\Delta/e=1.76k_bT_c/e=13.8$ mV the expected slope for rigid boundary junctions would be approximately $4.0\times10^5\ \mu$V. The fact that the slope of the line in Fig. 7 is only $1.31\times10^5\ \mu$V suggests that the superconducting gap is suppressed (as is expected for SNS junctions with soft boundary conditions) by a factor of 3, resulting in an effective gap $\Delta_i=4.5$ meV. The assumption of the BCS gap value for YBCO might represent an underestimation of the true gap value in the *a* or *b* directions and the suppression factor can therefore be even larger.

V. CONCLUSIONS

FEBI junctions have a number of unique properties that make them well suited for fundamental research into the nature of high-T_c junctions: (a) on-chip variation of barrier properties such as length and resistivity through controlled variation of the electron irradiation dose, (b) annealing of irradiated samples above room-temperature changes the electrical properties of the irradiated material enabling the study of the same junction with modified barrier properties. These properties combined with the fact that the junction can be fabricated in an unbroken single layer make it possible to systematically study junctions with a wide variety of barrier properties.

Based on the spread in damage estimated from the beam modulation experiment it was found that the shape of the damage distribution did not change significantly as a result of scanning the beam over an area. Rather, the large spatial spread of the beam, which leads to a barrier length of the order of 15 nm, meant that the dominant effect in the experiment was the increase of electron fluence received by the barriers. This increased fluence results in a higher resistance of the barrier while the barrier's spatial damage distribution remains nearly unchanged. The increased resistivity of the barrier and consequently smaller coherence length leads to a significant decrease of the critical current for SNS junctions in the dirty limit. This behavior can be quantitatively verified by checking whether the I_cR_n product at fixed temperature decreases exponentially with $R_n^{1/2}$. This behavior is found for all junctions after the same anneal stage with the exponent varying as $T^{1/2}$, as is expected for SNS junctions in the dirty limit.

Annealing reduces the R_n of junctions and leads to a significant increase of the I_c. This increase of the I_c cannot be explained by the decrease of resistance alone but is shown to be most likely the result of a simultaneously decreasing effective carrier mass or barrier length with increasing anneal temperature. If we assume a barrier length of 15 nm, the carriers' effective mass is of the order of 1 m_e.

Not only the scaling but also the magnitude of the critical current in FEBI junctions can be explained by SNS theory. The I_c close to T_c varies as $(T-T_c)^2$ as is expected for SNS junctions with soft boundary conditions. De Gennes' expression for the I_c using soft boundary conditions was found to describe the I_c data of all the junctions very well over a temperature range from 30 to 90.5 K. The parameter $L/\xi_{nd}(T_c)$ found from the fits to De Gennes' expression agreed well with the value found from the scaling of I_cR_n with R_n.

From the relation between the low-temperature I_cR_n data (4.2 K) and the ratio $L/\xi_{nd}(T_c)$ we find that the effective superconducting gap of the junctions at the SN interface is approximately a third of the BCS gap: $\Delta_i=4.5$ meV. One other discrepancy arises: the experimentally observed dependence suggests a maximum ratio for $L/\xi_{nd}(T_c)$ above which junctions no longer show a measurable I_cR_n product. These results clearly show that proximity coupling is a plausible mechanism for the Josephson effect observed in FEBI junctions.

ACKNOWLEDGMENTS

This work was supported in part by the European Union ESPRIT Program No. 7334 ''SUPACT.'' We would like to thank Dr. A. Hoole from the Engineering Department, University of Cambridge for his kind assistance with the STEM and Dr. D. A. Rudman and Dr. L. Vale of NIST, Boulder for providing us with the $YBa_2Cu_3O_{7-\delta}$ films.

[1] A. J. Pauza *et al.*, IEEE Trans. Appl. Supercond. **5**, 3410 (1995).
[2] S. K. Tolpygo *et al.*, Phys. Rev. B **53**, 12 462 (1996).
[3] B. A. Davidson *et al.*, Appl. Phys. Lett. **68**, 3811 (1996).
[4] L. Antagonazza *et al.*, Appl. Phys. Lett. **62**, 196 (1993).
[5] A. J. Pauza *et al.*, Physica B **194-196**, 119 (1993).
[6] A. Legris *et al.*, J. Phys. (France) I **3**, 1605 (1993).
[7] J. Giapintzakis *et al.*, Phys. Rev. B **50**, 15 967 (1994).
[8] S. K. Tolpygo *et al.*, Phys. Rev. B **53**, 12 454 (1996).
[9] P. G. De Gennes, Rev. Mod. Phys. **36**, 225 (1964).
[10] L. Antagonazza *et al.*, Phys. Rev. B **51**, 8560 (1995).
[11] K. Char, L. Antagonazza, and T. Geballe, Appl. Phys. Lett. **63**, 2420 (1993).
[12] A. W. Kleinsasser and K. A. Delin, Appl. Phys. Lett. **66**, 102 (1995).
[13] K. K. Likharev, Sov. Tech. Phys. Lett. **2**, 12 (1976).
[14] M. Y. Kupriyanov and V. F. Lukichev, Sov. J. Low. Temp. Phys. **8**, 526 (1982).
[15] M. G. Blamire *et al.*, IEEE Trans. Appl. Supercond. (to be published).
[16] B. A. Davidson *et al.* (unpublished).
[17] S. K. Tolpygo and M. Gurvitch (unpublished).
[18] D. J. v. Harlingen, Rev. Mod. Phys. **67**, 515 (1995).
[19] K. A. Delin and A. W. Kleinsasser, Supercond. Sci. Technol. **9**, 227 (1996).
[20] V. G. Kogan, Phys. Rev. B **26**, 88 (1982).
[21] V. G. Kogan and A. Y. Simonov, Phys. Rev. Lett. **68**, 2106 (1992).
[22] V. Z. Kresin and S. A. Wolf, *Fundamentals of Superconductivity* (Plenum, New York, 1990).
[23] A. T. Fiory *et al.*, Phys. Rev. Lett. **65**, 3441 (1990).
[24] B. Mayer *et al.*, Appl. Phys. Lett. **62**, 783 (1993).
[25] A. Barone and G. Patterno, *Physics and the Applications of the Josephson Effect* (Wiley, New York, 1982).
[26] A. J. Pauza *et al.*, Czech. J. Phys. **46**, 1325 (1996).
[27] G. Cliff, P. B. Kenway, and G. W. Lorimer, in *Analytical Electron Microscopy*, edited by D. B. Williams and D. C. Joy (San Francisco Press, San Francisco, 1984), p. 37.
[28] G. Cliff and P. B. Kenway, in *Microbeam Analysis*, edited by K. F. J. Heinrich (San Francisco Press, San Francisco, 1982), p. 107.